Developmental Cell, Volume *50*

Supplemental Information

Altering the Temporal Regulation of One Transcription Factor Drives Evolutionary Trade-Offs between Head Sensory Organs

Ariane Ramaekers, Annelies Claeys, Martin Kapun, Emmanuèle Mouchel-Vielh, Delphine Potier, Simon Weinberger, Nicola Grillenzoni, Delphine Dardalhon-Cuménal, Jiekun Yan, Reinhard Wolf, Thomas Flatt, Erich Buchner, and Bassem A. Hassan

Supplemental Information

Altering the temporal regulation of one transcription factor drives evolutionary trade-offs between head sensory organs

Ariane Ramaekers, Annelies Claeys, Martin Kapun, Emmanuèle Mouchel-Vielh, Delphine Potier, Simon Weinberger, Nicola Grillenzoni, Delphine Dardalhon-Cuménal, Jiekun Jan, Reinhard Wolf, Thomas Flatt, Erich Buchner, Bassem A. Hassan

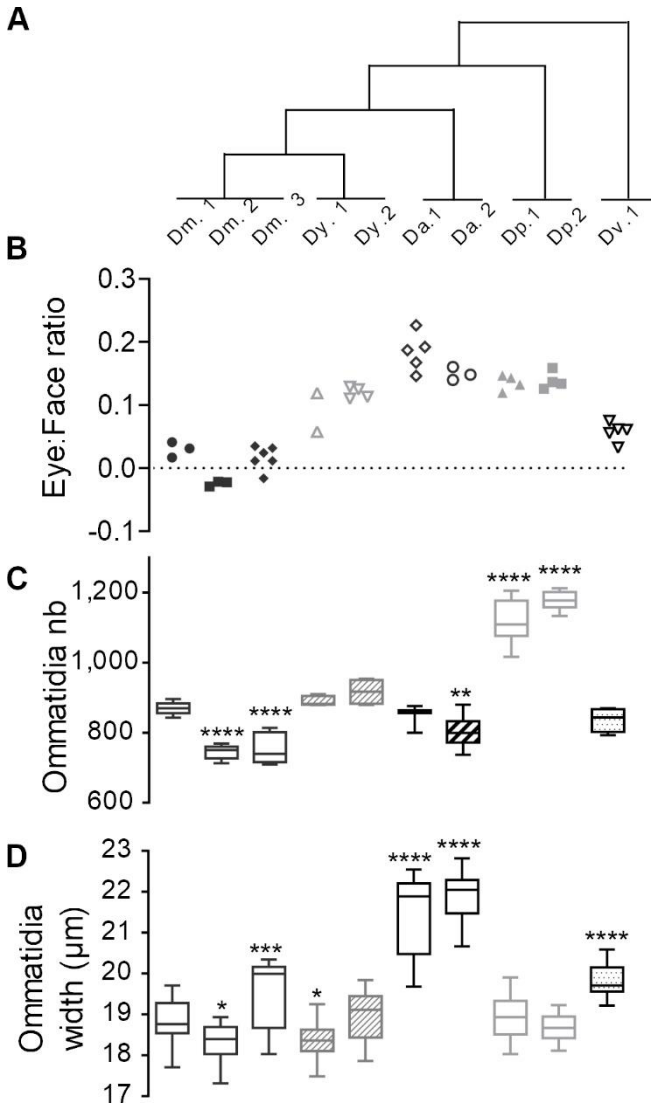

Figure S1. Natural variation in eye size in *Drosophila*, Related to Figure 1

(A to C') Eye size comparison between females from five *Drosophila* species: *D. melanogaster* (*D. mel.*), *D. yakuba* (*D. yak.*), *D. ananassae* (*D.ana.*), *D. pseudoobscura* (*D. pse.*), *D. virilis* (*D. vir.*). Different numbers indicate different strains (*see Methods*). Boxes indicate interquartile ranges, lines medians and whiskers data ranges.
(A) Phylogenic relationship between the five species (tree branches are not scaled).
(B) Eye: Face ratio measured from SEM images.
(C) Ommatidia number counted on SEM images. Ordinary one-way ANOVA **** *p<0.0001* followed by Dunnett's multiple comparisons. See also Table S1.
(D**)** Ommatidia width. Ordinary one-way ANOVA **** *p<0.0001* followed by Dunnett's multiple comparisons. See also Table S1
For this experiment, flies were raised at 21°C.

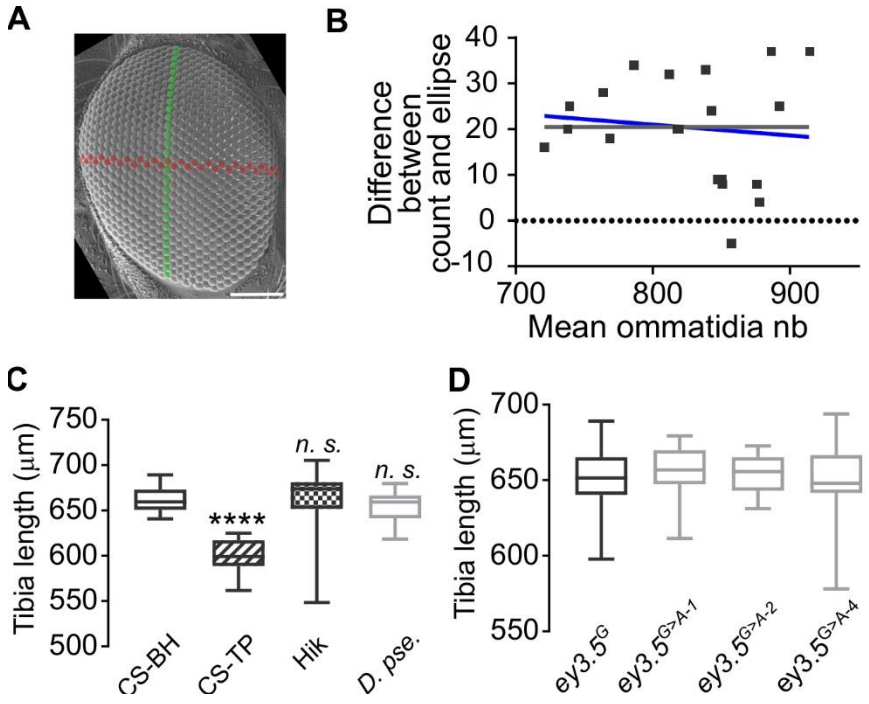

Figure S2. Ommatidia number variation: scaling and methods, Related to Figures 1, 4 and 6

(A) SEM image of a *D. mel.* Hikone-AS eye. *Green*: dorso-ventral axis; *Red*: anterior-posterior axis. Scale bar: 100 µm.
(B) Bland-Altman chart plotting the difference in ommatidia number measured by two methods (ellipse-based estimation vs direct counting) over their mean (Bland and Altman, 1986). Comparison of fits indicates that the difference between the two measurements is independent of the mean (null hypothesis, grey line: slope= 0.0; alternative hypothesis blue line: slope unconstrained = -0.02372; *p=0.6212*).
(C) Mesothoracic tibia (T2) length in three wild-type *D. mel.* stocks (Canton-S^{BH}, Canton-S^{TP}, Hikone-AS) and *D. pse.*.
Sample sizes from left to right (n=21, n=23, n=29, n=21). Kruskal Wallis test **** *p<0.0001* followed by Dunn's multiple comparisons: **** *p<0.0001*; *n.s. p>0.9999.*
(D) Mesothoracic tibia (T2) length in CRISPR/Cas9 engineered and control lines. Sample sizes (n=20). Ordinary One way ANOVA *n.s. p=0.7600.*

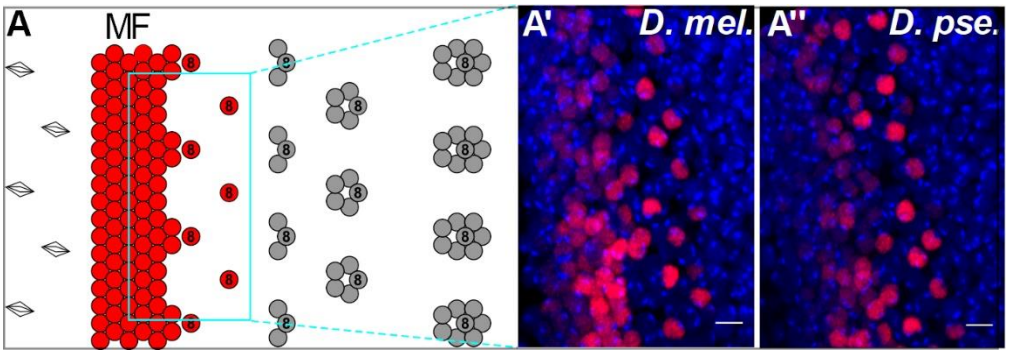

Figure S3. Developmental origin of eye size variation in *D. mel.* and *D. pse*., Related to Figure 2

(A) Schematics of the first steps of retinal differentiation showing the singling-out of committed Ato-expressing R8 ommatidia progenitor cells and subsequent steps of ommatidia assembly.

(A' and A'') The density of Ato-expressing R8 progenitors (in red in A' and A'') is similar in the two species. *Red*: anti-Ato immunostaining; *blue*: DAPI. Anterior is at the left. Scale bars: 5 μm.

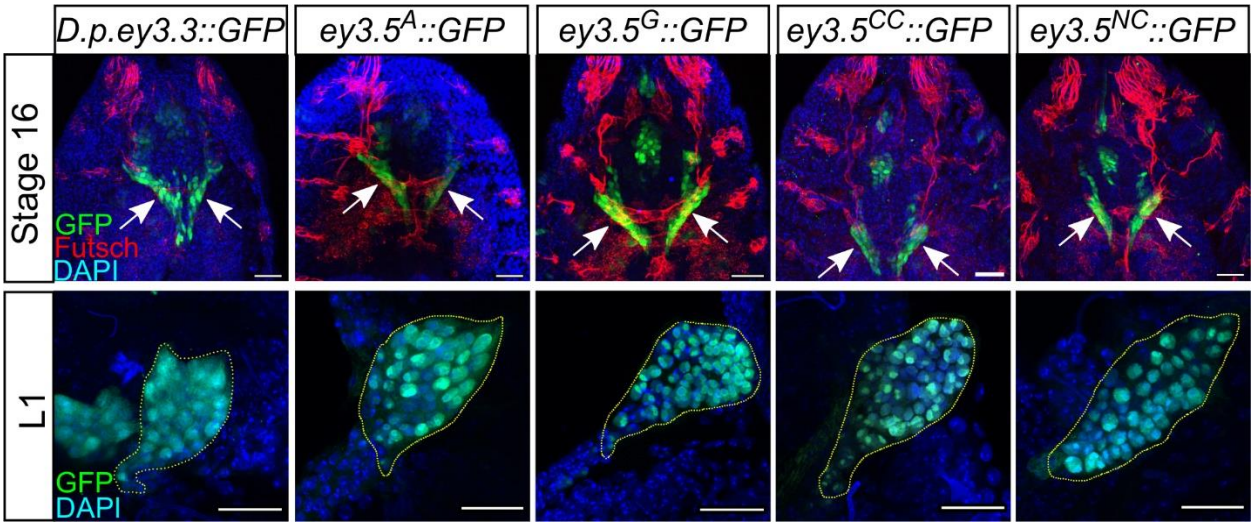

Figure S4. Eyeless enhancer activity in early EADs. Related to Figure 3 and Figure 4.

The *D. pse*. and the four *D. mel.* alleles of the *ey* eye enhancer drive GFP expression in the entire EAD in stage 16 embryos (arrows in upper panel) and in 1st instar larvae (L1; yellow dashed line in lower panel). Green: GFP; Blue: DAPI; Red: anti-Futsch (22C10). Scale bars: 20 μm.

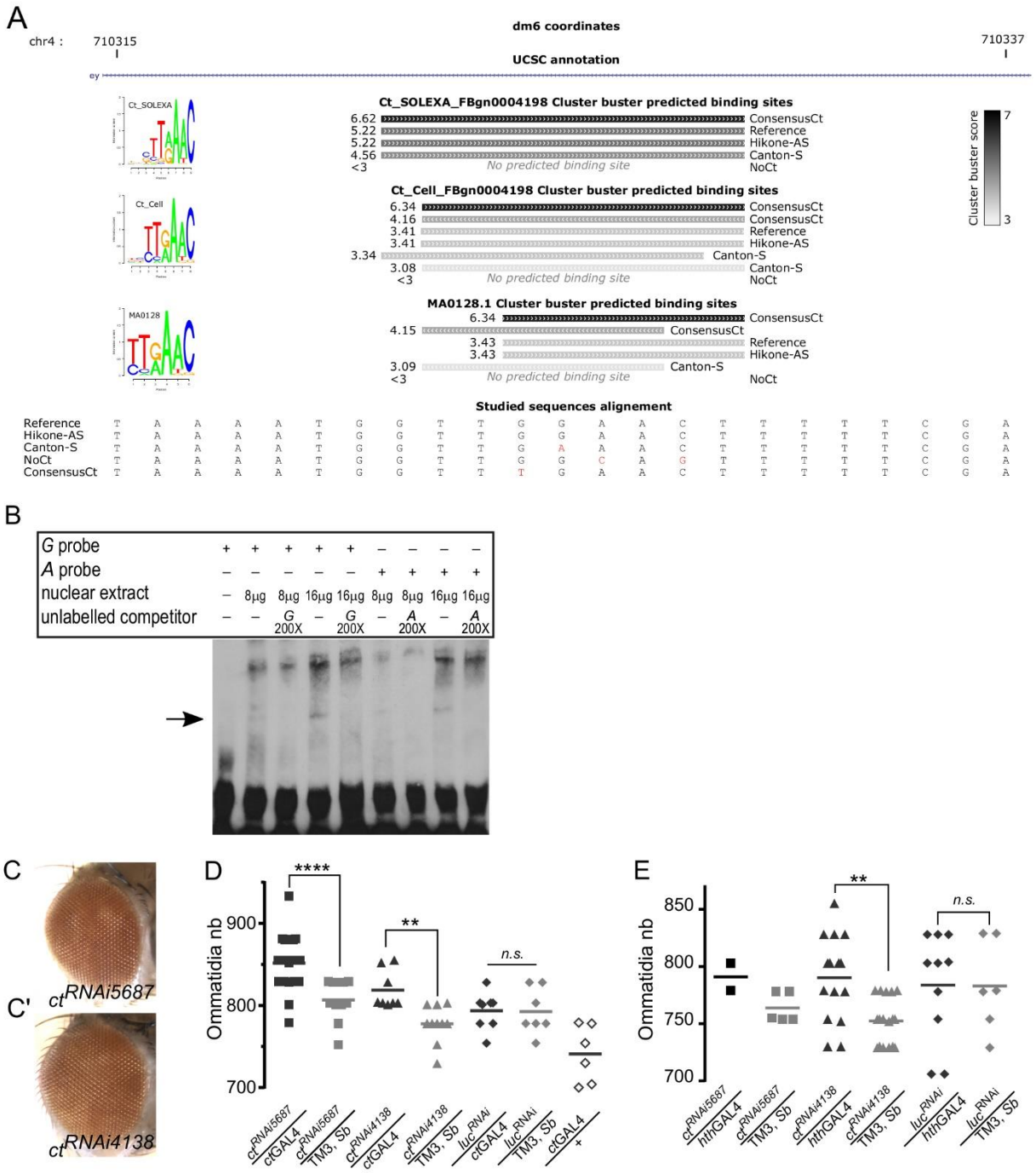

Figure S5: Ct TF binds *ey* enhancer and regulates eye size, Related to Figure 4.

(A) Visualization of Cluster-Buster Ct predicted binding sites for natural and synthetic *ey* enhancer alleles at the SNP location. Scores are represented by a grey scale. PWMs corresponding sequence logos plotted by seqLogo (https://rdrr.io/bioc/seqLogo/) are shown on the left.

(B) Electrophoretic mobility shift assay. The Cut-FLAG nuclear extract induces a band shift (black arrow) with oligonucleotide probes corresponding to both *G* and *A*-enhancer alleles. Both shifts are eliminated when corresponding non-labeled competitors are added.

(C and C') RNAi-mediated KD of *ct* using two distinct RNAi constructs does not induce gross morphology defects in the compound eye. Gal4 driver: *ctGal4*.

(D) Overexpression of two UAS-ct^{RNAi} and one UAS-$luciferase^{RNAi}$ constructs under the control of *ct*GAL4. Sample sizes from left to right (n=23, n=13, n=8, n=10, n=8, n=7, n=6). Ordinary one-way ANOVA **** *p<0.0001* followed by Sidak's multiple comparisons: $ct^{RNAi5687}$/*ctGal4* vs $c^{tRNAi5687}$/ TM3, Sb **** *p<0.0001*; $ct^{RNAi5687}$/*ctGal4* vs *ctGAL4*/ + **** *p<0.0001;* $ct^{RNAi4138}$/*ctGal4 vs* $ct^{RNAi4138}$/TM3, Sb * *p=0.0126*; $ct^{RNAi4138}$/*ctGal4 vs ctGAL4*/ + **** *p<0.0001;* luc^{RNAi} /*ctGal4* vs luc^{RNAi} / TM3, Sb *n. s. p>0.9999;* luc^{RNAi} /*ctGal4 vs ctGAL4*/ + ** *p=0.0036*.

(E) Overexpression of two UAS-*ct*RNAi and one UAS-*luciferase*RNAi constructs under the control of *hth*GAL4. Sample sizes, from left to right (n=2, n=5, n=15, n=17, n=10, n=7). Sample size for ctRNAi5687/hthGAL4 was low due to the lethality or gross morphological defects caused by this allelic combination. Ordinary one-way ANOVA ** *p=0.0089* followed by Sidak's multiple comparisons: $ct^{RNAi4138}$/*hthGal4 vs* $ct^{RNAi4138}$/TM3, Sb ** *p=0.0047;* luc^{RNAi} /*hthGal4* vs luc^{RNAi} / TM3, Sb *n. s. p=0.2152*.

(D and E) Scatter dot plots. Line indicates the mean.

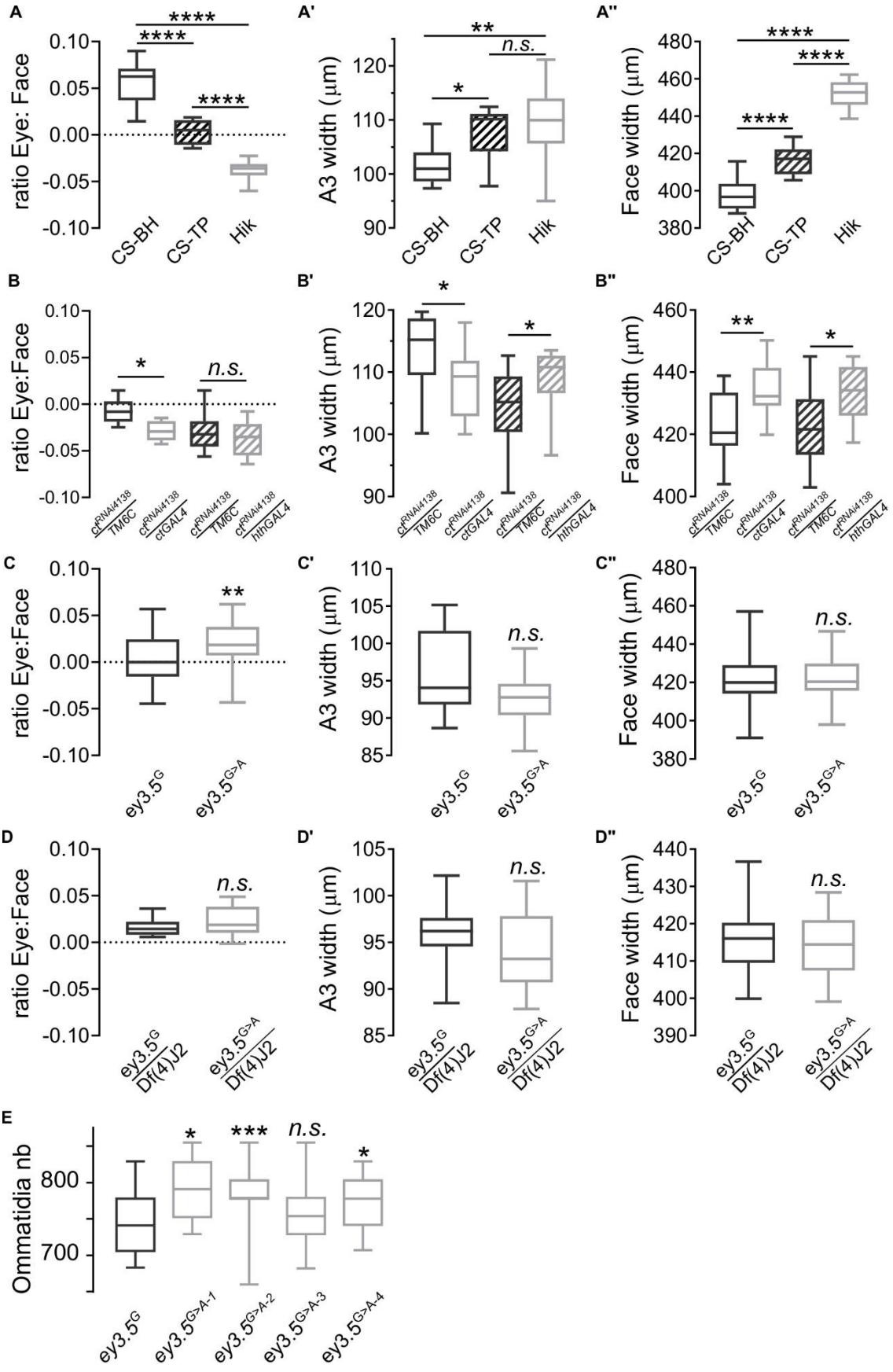
A
A'
A''
ratio Eye: Face
A3 width (µm)
Face width (µm)
CS-BH
CS-TP
Hik
B
B'
B''
ratio Eye:Face
ctRNAi4138/TM6C
ctRNAi4138/ctGAL4
ctRNAi4138/hthGAL4
C
C'
C''
ey3.5G
ey3.5G>A
D
D'
D''
ey3.5G/Df(4)J2
ey3.5G>A/Df(4)J2
E
Ommatidia nb
ey3.5G
ey3.5G>A-1
ey3.5G>A-2
ey3.5G>A-3
ey3.5G>A-4
n.s.

Figure S6. Eye: Face ratio, absolute A3 width and absolute face width. Related to Figure 4, Figure 6 and Figure S5.

Boxes indicate interquartile ranges, lines medians and whiskers data ranges.

(A) Sample sizes (n=12, n=14, n=10). Ordinary one-way ANOVA **** *p<0.0001* followed by Tukey's multiple comparisons: **** adjusted *p<0.0001*.

(A') Sample sizes (n=11, n=11, n=13). Ordinary one-way ANOVA ** *p=0.0035* followed by Tukey's multiple comparisons: ** adjusted *p=0.0043*; * adjusted *p = 0.0184*; *n.s* adjusted *p=0.7600*.

(A'') Sample sizes (n=12, n=14, n=10). Ordinary one-way ANOVA **** *p<0.0001* followed by Tukey's multiple comparisons: **** adjusted *p<0.0001*.

(B) Sample sizes (n=19, n=19, n=12, n=12). Unpaired t-tests: **** *p<0.0001*; *n.s. p=0.37831*.

(B') Sample size (n=12). Unpaired t-tests: * *p=0.0288*; * *p=0.0444*.

(B'') Sample sizes (n=13, n=13, n=12, n=12). Unpaired t-tests: ** *p=0.0042*; * *p=0.0163*.

(C) Sample size (n=42). Unpaired t-tests: ** *p=0.0060*.

(C') Sample sizes (n=16, n=14). Unpaired t-tests: *n.s. p=0.0553*.

(C'') Sample size (n=42). Unpaired t-tests: *n.s. p=0.5831*.

(D) Sample sizes (n=9; n=16). Unpaired t-tests: *n.s. p=0.2625*.

(D') Sample sizes (n=9; n=16). Unpaired t-tests: *n.s. p=0.2220*.

(D'') Sample sizes (n=9; n=16). Unpaired t-tests: *n.s. p=0.5353*.

(E) Estimated ommatidia numbers in control *G*-carrying and the four CRISPR engineered *A*-carrying variants imaged by light microscopy. Sample sizes: from left to right (n=24, n=8, n=32, n=33, n=45); Ordinary one-way ANOVA *** *p=0.0009* followed by Dunnet's multiple comparisons between the control and the four CRISPR lines.

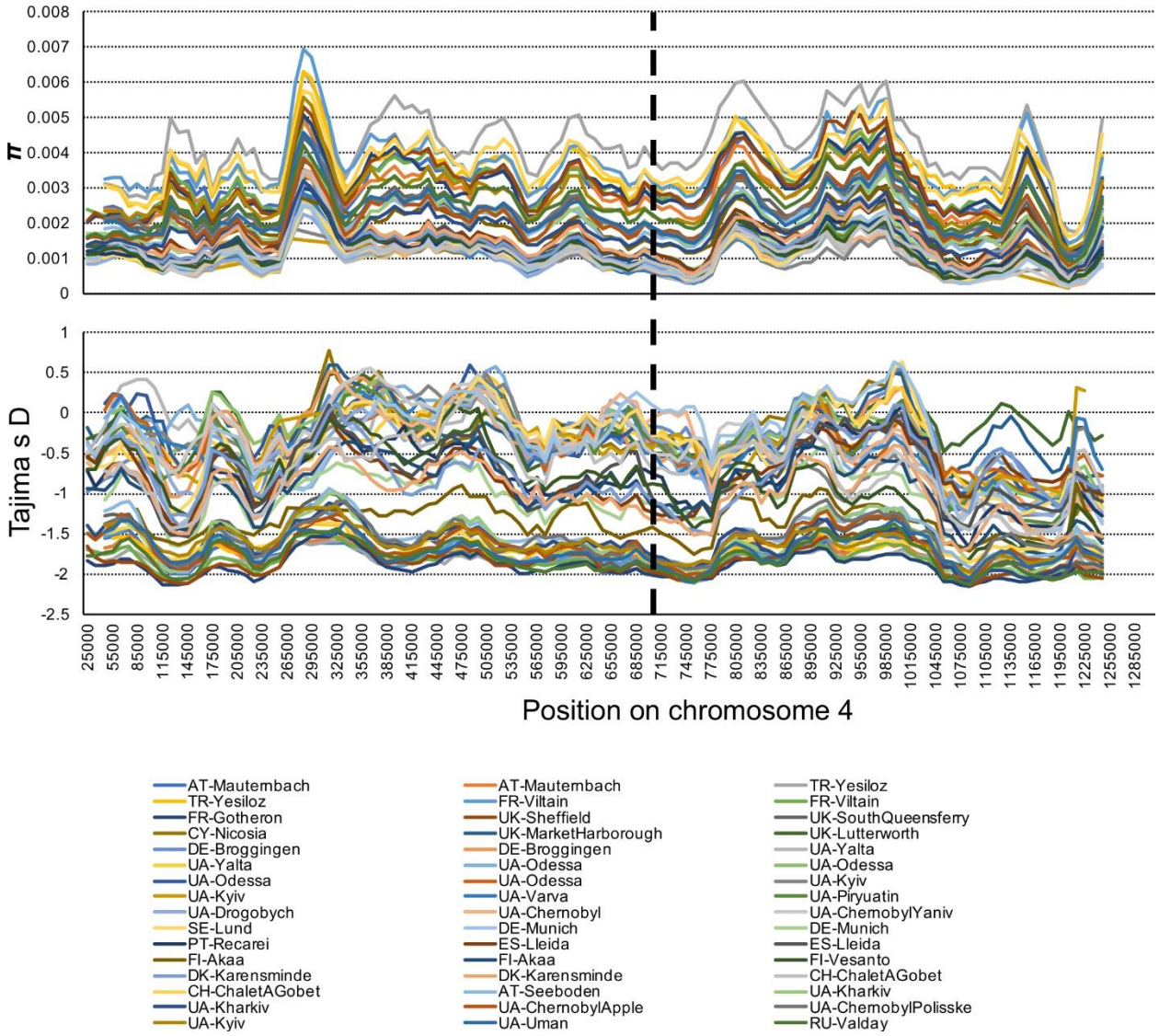

Figure S7. Genetic variation of the fourth chromosome in Europe, Related to Figure 5

The distribution of π (top panel) and Tajima's *D* (bottom panel) in 50kb windows with 10kb step-size for 48 population samples from Europe. The vertical dashed black line indicates the approximate genomic position of the focal SNP at position Chr 4: 710326.

Table S1. Natural variation in *Drosophila* eye size, Related to Figures 1, S1.

Genotype	Ommatidia Number		Ommatidia width	
	n	***adjusted p value***	**n**	**adjusted *p* *value***
D. m. 2	n=7	*p = 0.0001*	n=24	*p = 0.0161*
D. m. 3	n=8	*p = 0.0001*	n=24	*p = 0.0002*
D. y. 1	n=5	*p = 0.9396*	n=24	*p = 0.0462*
D. y. 2	n=4	*p = 0.2764*	n=24	*p = 0.9922*
D. a. 1	n=8	*p = 0.9770*	n=24	*p = 0.0001*
D. a. 2	n=8	*p = 0.0083*	n=24	*p = 0.0001*
D. p. 1	n=9	*p = 0.0001*	n=24	*p = 0.9994*
D. p. 2	n=8	*p = 0.0001*	n=24	*p = 0.9072*
D. v.	n=4	*p = 0.6782*	n=24	*p = 0.0001*

Sample sizes and results of Dunnett's multiple comparison tests following ordinary one-way ANOVA from Figure S1. Comparisons towards *D. m. 1* (Canton-S^{BH}; ommatidia number sample size n=6; ommatidia width sample sizes n=24).

Table S2. Ct binding site predictions at the SNP location, Related to Figure 4

Data are presented in a separate Excel document.

Predictions of Ct binding sites in a 1 kb region surrounding the SNP at position Chr 4: 710326 (500 bp up and down) scored with Cluster-Buster (Frith et al., 2003).

Table S3. Worldwide allele frequency patterns, Related to Figure 5

Country	Location	Data Type	Data Reference	Frequency
Australia	Sorell	Pool	Reinhardt et al. 2012	0.206
Australia	Queensland	Pool	Reinhardt et al. 2012	0.081
Austria	Gross-Enzersdorf	Pool	Bergland et al. 2014; Kapun et al. 2016	0.159
Cameroon	Oku	Single	Pool et al. 2012	0.000
China	Beijing	Single	Grenier et al. 2015	0.070
Egypt	Cairo	Single	Lack et al. 2015	0.088
Ethiopia	Gambella	Single	Lack et al. 2015	0.000
Ethiopia	Fiche	Single	Lack et al. 2015	0.000
France	Lyon	Single	Pool et al. 2012	0.011
Gabon	Franceville	Single	Pool et al. 2012	0.000
Malawi	Mwanza	Single	Langley et al. 2012	0.000
Netherlands	Houten	Single	Grenier et al. 2015	0.000
Rwanda	Gikongoro	Single	Pool et al. 2012	0.000
Spain	Barcelona	Pool	Bergland et al. 2014; Kapun et al. 2016	0.012
USA	Homestead	Pool	Bergland et al. 2014; Kapun et al. 2016	0.091
USA	Hahira	Pool	Bergland et al. 2014; Kapun et al. 2016	0.154
USA	Eutawville	Pool	Bergland et al. 2014; Kapun et al. 2016	0.056
USA	Raleigh	Pool	Bergland et al. 2014; Kapun et al. 2016	0.000
USA	Charlottesville	Pool	Bergland et al. 2014; Kapun et al. 2016	0.055
USA	Winters	Single	Campo et al. 2013	0.286
USA	Linvilla	Pool	Bergland et al. 2014; Kapun et al. 2016	0.100
USA	Ithaca	Pool	Bergland et al. 2014; Kapun et al. 2016	0.156
USA	Lancaster	Pool	Bergland et al. 2014; Kapun et al. 2016	0.230
USA	Cross Plains	Pool	Bergland et al. 2014; Kapun et al. 2016	0.112
USA	Bowdoinham	Pool	Bergland et al. 2014; Kapun et al. 2016	0.000
Zambia	Siavonga	Single	Pool et al. 2012	0.000
Cyprus	Nicosia	Pool	Kapun et al. 2018	0.013

Turkey	Yesiloz	Pool	Kapun et al. 2018	0.000
Turkey	Yesiloz	Pool	Kapun et al. 2018	0.019
Portugal	Recarei	Pool	Kapun et al. 2018	0.034
Spain	Lleida	Pool	Kapun et al. 2018	0.000
Spain	Lleida	Pool	Kapun et al. 2018	0.029
Ukraine	Yalta	Pool	Kapun et al. 2018	0.000
Ukraine	Yalta	Pool	Kapun et al. 2018	0.000
France	Gotheron	Pool	Kapun et al. 2018	0.128
Ukraine	Odessa	Pool	Kapun et al. 2018	0.000
Ukraine	Odessa	Pool	Kapun et al. 2018	0.000
Ukraine	Odessa	Pool	Kapun et al. 2018	0.000
Ukraine	Odessa	Pool	Kapun et al. 2018	0.000
Switzerland	ChaletAGobet	Pool	Kapun et al. 2018	0.096
Switzerland	ChaletAGobet	Pool	Kapun et al. 2018	0.081
Austria	Seeboden	Pool	Kapun et al. 2018	0.055
Germany	Munich	Pool	Kapun et al. 2018	0.045
Germany	Munich	Pool	Kapun et al. 2018	0.021
Germany	Broggingen	Pool	Kapun et al. 2018	0.052
Germany	Broggingen	Pool	Kapun et al. 2018	0.090
Austria	Mauternbach	Pool	Kapun et al. 2018	0.053
Austria	Mauternbach	Pool	Kapun et al. 2018	0.029
Ukraine	Uman	Pool	Kapun et al. 2018	0.000
France	Viltain	Pool	Kapun et al. 2018	0.029
France	Viltain	Pool	Kapun et al. 2018	0.131
Ukraine	Drogobych	Pool	Kapun et al. 2018	0.000
Ukraine	Kharkiv	Pool	Kapun et al. 2018	0.000
Ukraine	Kharkiv	Pool	Kapun et al. 2018	0.000
Ukraine	Piryuatin	Pool	Kapun et al. 2018	0.000
Ukraine	Kyiv	Pool	Kapun et al. 2018	0.000
Ukraine	Kyiv	Pool	Kapun et al. 2018	0.071
Ukraine	Kyiv	Pool	Kapun et al. 2018	0.024
Ukraine	Varva	Pool	Kapun et al. 2018	0.000
Ukraine	ChernobylApple	Pool	Kapun et al. 2018	0.020
Ukraine	ChernobylPolisske	Pool	Kapun et al. 2018	0.015
Ukraine	Chernobyl	Pool	Kapun et al. 2018	0.000
Ukraine	ChernobylYaniv	Pool	Kapun et al. 2018	0.036
UK	Lutterworth	Pool	Kapun et al. 2018	0.078
UK	MarketHarborough	Pool	Kapun et al. 2018	0.072
UK	Sheffield	Pool	Kapun et al. 2018	0.011

Sweden	Lund	Pool	Kapun et al. 2018	0.121
Denmark	Karensminde	Pool	Kapun et al. 2018	0.019
Denmark	Karensminde	Pool	Kapun et al. 2018	0.000
UK	SouthQueensferry	Pool	Kapun et al. 2018	0.173
Russia	Valday	Pool	Kapun et al. 2018	0.000
Finland	Akaa	Pool	Kapun et al. 2018	0.048
Finland	Akaa	Pool	Kapun et al. 2018	0.018
Finland	Vesanto	Pool	Kapun et al. 2018	0.000

Origin, data type, data source and allele frequencies of the *A*-variant of the focal SNP at position Chr 4: 710326 of world-wide populations with sample sizes ≥ 10 individuals.

Table S4. Isofemale line genotypes, Related to Figure 5

Data are presented in a separate Excel document.

Genotypes and admixture status for isofemale lines from Sub-Saharan Africa.

Table S5. List of oligonucleotides, Related to Star Methods

name	sequence	used for
ey3.3Pse_F	GGGGACAAGTTTGTACAAAAAAGCAGGCTAAGTGGTAGTGGACTAGG	cloning of ey enhancer
ey3.3Pse_R	GGGGACCACTTTGTACAAGAAAGCTGGGTCCTAGAATTTTGCTAACGC	cloning of ey enhancer
ey3.5Mel_F	GGGGACAAGTTTGTACAAAAAAGCAGGCTGGACTAGGCGGTATTGCT	cloning of ey enhancer
ey3.5Mel_F	GGGGACCACTTTGTACAAGAAAGCTGGGTTTTGCTCACACATCCATTTG	cloning of ey enhancer
ey3.5NoCt_F	caataaaatggttgg**C**a**G**ttttcgaactttcg	site directed mutation of ey enhancer
ey3.5NoCt_R	cgaaagttcgaaaaa**C**t**G**ccaaccattttattg	site directed mutation of ey enhancer
ey3.5ConsensusCt_F	taaaatggtt**T**gaacttttcgaactttcg	site directed mutation of ey enhancer
ey3.5ConsensusCt_R	gaaaaagttcAaaccattttattgttttc	site directed mutation of ey enhancer
ey3.5gRNA_F	phospho-CTTCgtcgaaaacaataaaatggt	guideRNA construct
ey3.5gRNA_R	phospho-AAACaccattttattgttttcgaC	guideRNA construct
ey_R3	agaaatatcacatggccgag	allele-specific PCR
ey-SNPG-F	ggaatcgaaaacaataaaatgg**c**tg**g**	allele-specific PCR
Ey-SNP^{A}-F	ggaatcgaaaacaataaaatggctg**a**	allele-specific PCR
EMSA_G	ACAATAAAATGGTTGGAACTTTTTCGAACTTT	EMSA
EMSA_A	ACAATAAAATGGTTGAAACTTTTTCGAACTTT	EMSA